

---

# Enhancing Hierarchical Information by Using Metric Cones for Graph Embedding

---

Daisuke Takehara<sup>1</sup> Kei Kobayashi<sup>1</sup>  
Abstract

Graph embedding is becoming an important method with applications in various areas, including social networks and knowledge graph completion. In particular, Poincaré embedding has been proposed to capture the hierarchical structure of graphs, and its effectiveness has been reported. However, most of the existing methods have isometric mappings in the embedding space, and the choice of the origin point can be arbitrary. This fact is not desirable when the distance from the origin is used as an indicator of hierarchy, as in the case of Poincaré embedding. In this paper, we propose graph embedding in a metric cone to solve such a problem, and we gain further benefits: 1) we provide an indicator of hierarchical information that is both geometrically and intuitively natural to interpret, 2) we can extract the hierarchical structure from a graph embedding output of other methods by learning additional one-dimensional parameters, and 3) we can change the curvature of the embedding space via a hyperparameter.

## 1. Introduction

In recent years, machine learning for graph-structured data has attracted significant attention. A recently developed method is using graph convolutional neural networks (Kipf & Welling, 2017), which apply convolutional neural networks to graphs. In this study, we focus on graph embedding, which has become an important method with applications in social networks (Hoff et al., 2002), knowledge graph completion (Bordes et al., 2013), and other fields. In particular, various methods of embedding in non-Euclidean spaces have been proposed to capture the hierarchical structure of graphs. In (Klimovskaia et al., 2020), Poincaré embedding (Nickel & Kiela, 2017) has been applied to extract hierarchies from biological cell data.

However, there are three major problems with existing graph embedding methods that are used for extracting the hierarchical structures.

The first problem concerns the selection of the origin point. The distance from the origin is used as an indicator of hierarchy when applying the embedding method to the space where an isometric map exists. In non-Euclidean spaces, existing graph embedding methods use a loss function that depends on the distance between two nodes in the embedding. Because the distance from the origin is changed by the isometric transformation as the value of the loss function is not changed, it is not appropriate to use the distance from the origin as an indicator of hierarchy. In other words, when we define the indicator of the hierarchy in the space where the isometric map exists, it is necessary to be invariant to the isometric map.

The second problem is a lack of scalability. If we are interested in information other than the hierarchical structure in the existing methods for hierarchical embedding, we need to learn another embedding or solve the problem by an independent method because the embedding does not consider that information. Therefore, we cannot directly apply the embedding method using non-Euclidean space for extracting the hierarchical structure.

The third problem is that the curvature of the space needs to be considered in graph embedding in non-Euclidean spaces. For example, because the curvature of the Poincaré sphere changes depending on the scaling of the space, the embedding result may change if the scaling is varied.

In this paper, we propose a method of embedding graphs in metric cones as a solution to the three problems described above. A metric cone can be defined on any length metric space—a wide class of metric spaces (including normed vector spaces, manifolds, and metric graphs). This space’s dimension is larger than that of the original space. It is known that the curvature

---

The first author was supported by RIKEN AIP Japan. The second author was supported by JSPS KAKENHI (JP19K03642, JP19K00912) and RIKEN AIP Japan. <sup>1</sup>Faculty of Science and Technology, Keio University, Yokohama, Japan.

of this space can be varied, and a method of changing the structure of the data space for analysis has also been proposed (Kobayashi & Wynn, 2020).

First, we show that it is effective to use the coordinate corresponding to “the height of the metric cone” (a one-dimensional parameter added to the original space) as an indicator of hierarchy. Second, we demonstrate that the hierarchical structure can be extracted by learning the embedding of the metric cone, which optimizes the only one-dimensional parameter, in case we have a graph embedding pretrained. By keeping the coordinates of the original space fixed, we show that only the one-dimensional parameter corresponding to the height of the cone is learned, and the computation time is reduced. Additionally, if we use the Euclidean model for the pretrained embedding, we show that our model is scalable to solving other tasks, preserving the original space structure. Third, we show that the curvature can be optimized for the data by taking advantage of the fact that the curvature of the embedding space can be varied. The curvature of a metric cone varies with one parameter that corresponds to the generatrix of the cone. If we have the pretrained embedding, we show that the learning method is also computationally efficient, because curvature can be optimized by learning one-dimensional parameters without changing the structure of the original space (i.e., without learning the embedding in the original space).

The remainder of this paper is organized as follows. Section 2 describes related research. In Section 3, we propose the method of graph embedding in a metric cone, with the introduction of 1) graph embedding in non-Euclidean spaces and 2) the definition and properties of metric cones. Section 4 presents the experimental results using graph data, followed by a conclusion and future perspectives in Section 5.

## 2. Related Work

### 2.1. Random Walk Models

DeepWalk (Perozzi et al., 2014) samples series by random walks on graphs and applies a method for embedding series data, such as the skip-gram model (word2vec (Mikolov et al., 2013)). The sampling method of DeepWalk’s random walk series has been modified to depend on edge weights in node2vec (Grover & Leskovec, 2016), and a method that simultaneously optimizes hyperparameters (such as random walk length) has been proposed in (Abu-El-Haija et al., 2018). Unlike our proposed method, these methods were not designed to represent a hierarchical structure but were simply designed to embed the structure of a graph with high accuracy, which is evaluated by predicting edge links.

### 2.2. Dimensionality Reduction Models

Dimensionality compression methods exist for data in Euclidean space, such as multidimensional scaling (MDS) (Kruskal, 1964), IsoMAP (Tenenbaum et al., 2000), and locally linear embedding (LLE) (Roweis & Saul, 2000). By applying it to the adjacency matrix of a graph, an embedded representation of the graph can be obtained. There are also methods to obtain an embedded representation of a graph by applying dimensionality reduction to the graph’s Laplacian matrix (Belkin & Niyogi, 2002) instead of the adjacency matrix. As an alternative to random walk models, these graph embedding methods are also used to accurately embed the structure of the graph but not to represent a hierarchical structure.

### 2.3. Graph Neural Networks

Methods to compress dimensionality of adjacency matrices (Cao et al., 2016)(Wang et al., 2016) or the graph’s Laplacian matrices (Kipf & Welling, 2016) using a neural network (autoencoder) to obtain a representation of the graph embedding have been proposed. These methods can be easily applied to other tasks. However, as with the above categories, these methods are designed for simply embedding the structure of a graph but not for representing a hierarchical structure.

### 2.4. Non-Euclidean Models (Hyperbolic Embedding Models)

Poincaré embedding (Nickel & Kiela, 2017) is a method to embed the adjacency matrix of a graph in a skip-gram model, large-scale information network embedding (LINE) (Tang et al., 2015), which is constructed on a Poincaré sphere. In addition, there are other methods to embed graphs into Lorentz models (Nickel & Kiela, 2018) and to embed each node of a graph as a cone instead of a point (Ganea et al., 2018). These methods exist to describe the hierarchy of each graph according to the inclusion relation of the cones. In previous research, the hierarchical structure could be accurately captured, but the problem of invariance for isometric maps prevented the natural definition of a metric that would represent the hierarchical structure. Therefore, embedding parameters in non-Euclidean spaces makes them difficult to use in other

tasks. In contrast, our proposed method can use a Euclidean embedded representation of all parameters except for the one-dimensional parameters. The purpose is to provide an embedding method that is easy to use for other tasks and provides a natural indicator of hierarchical information.

### 3. Methods

From this point onwards, the set of edges in an undirected graph  $G$  is denoted by  $E$ , the set of vertices by  $V$ , and the embedded space by  $X$ .

#### 3.1. Graph Embedding in Non-Euclidean Spaces

Following Poincaré embedding, we learn the embedding of a graph  $G$  by maximizing the following objective function:

$$L = \sum_{(u,v) \in E} \log \frac{\exp(-d(u,v))}{\sum_{v' \in N(u)} \exp(-d(u,v'))}, \quad (1)$$

where  $N(u) : \{v' \in V | (u, v') \notin E\}$  denotes the set of points not adjacent to node  $u$  (including  $u$  itself), and  $d$  denotes the distance function of the embedded space (for Poincaré embedding and the Poincaré sphere). We can say that this objective function is a negative sampling approximation of a model in which the similarity is  $-1$  times the distance, and the probability of the existence of each edge is represented by a SoftMax function on the similarity:

$$\begin{aligned} \sum_{(u,v) \in E} \log \frac{\exp(-d(u,v))}{\sum_{v' \in V} \exp(-d(u,v'))} \\ \approx \sum_{(u,v) \in E} \log \frac{\exp(-d(u,v))}{\sum_{v' \in N(u)} \exp(-d(u,v'))}. \end{aligned} \quad (2)$$

The maximization of the objective function is done by stochastic gradient descent on Riemannian manifolds (Riemannian SGD). The stochastic gradient descent over the Euclidean space updates the parameters as follows:

$$u \leftarrow u - \eta \nabla_u L(u), \quad (3)$$

where  $\eta$  is the learning rate. However, in non-Euclidean, the sum of vectors is not defined, and  $\nabla_u L(u)$  is the point of the tangent space  $T_u X$  of  $u$ ; hence, SGD cannot be applied. Therefore, we update the parameters by using an exponential map instead of the sum:

$$u \leftarrow \exp_u(-\eta \nabla_u^R L(u)). \quad (4)$$

With the metric of the embedding space as  $g_u(u \in V)$ , the gradient on the Riemannian manifold  $\nabla_u^R L(u)$  is the scaled gradient in the Euclidean space:

$$\nabla_u^R L(u) = g_u^{-1} \nabla_u L(u). \quad (5)$$

#### 3.2. Metric Cone

The metric cone is similar to ordinary cones (e.g. circle cones) in the sense that it is defined as a collection of line segments connecting an apex point to a given set. However, the metric cone has a notable property such that every point in the original set is embedded at an equal distance from the apex point and this is a desirable property for hierarchical structure extraction.

The metric cone has been studied as an analogy to the length metric spaces of the tangent cone for differential manifolds with singularities. Length metric space is a metric space where the distance between any two points is equal to the shortest curve length connecting them. Length metric space includes Euclidean spaces, normed vector spaces, manifolds (e.g., Poincaré ball; sphere), metric graphs, and many other metric spaces. Assume the original space  $Z$  is a length metric space, then the metric cone generated by  $Z$  is  $X := Z \times [0, 1] / Z \times \{0\}$  with a distance function determined as follows:

$$\begin{aligned} \bar{d}_\beta((x, s), (y, t)) \\ = \beta \sqrt{t^2 + s^2 - 2ts \cos(\pi \min(d_Z(x, y)/\beta, 1))} \end{aligned} \quad (6)$$

where  $\beta > 0$  is a hyperparameter corresponding to the length of the conical generatrix. Note that the metric cone itself also becomes a length metric space, and it embeds the original space (i.e., the space is one dimension larger than the original space). The distance in the metric cone corresponds to the length of the shortest curve on the circle section (blue line segment(s) in the right two subfigures in Figure 1) whose bottom circumference is the distance of the original space  $Z$  and whose radius is  $\beta$ .

When the curvature is measured in the sense of  $\text{CAT}(k)$  property, a curvature measure for general length metric spaces, the curvature value  $k$  can be controlled by  $\beta$ . Other properties of the metric cone are examined in (Sturm, 2003), (Deza & Deza, 2009). Because the metric cone can change the curvature of the space by changing parameter  $\beta$ , its usefulness has been reported in an analysis using the structure of the data space (Kobayashi & Wynn, 2020).

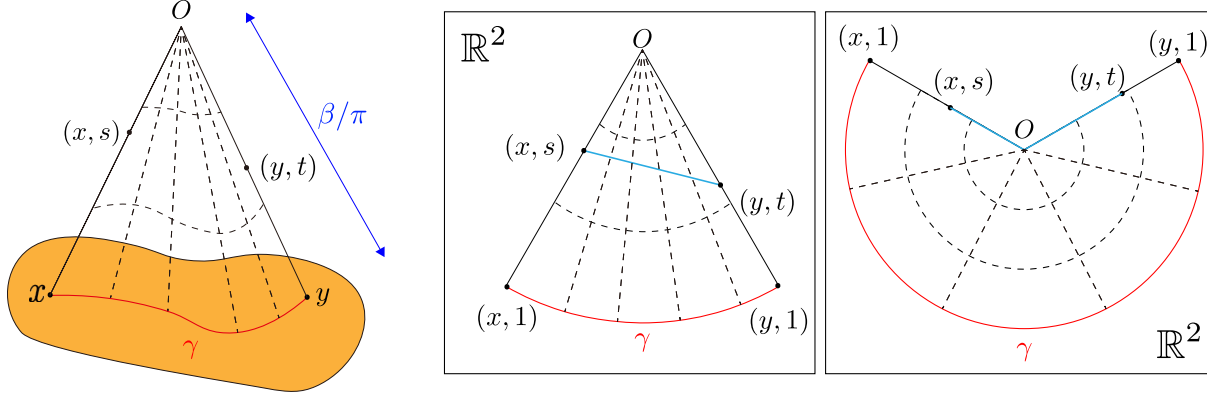


Figure 1. The Left figure depicts a conceptual image of an original space and its metric cone. A circle section to compute the distance in the metric cone is depicted in the middle figure (when the apex angle  $< \pi$ ) and the right figure (when the apex angle  $\geq \pi$ ).

The metric  $\bar{g}$  of a metric cone is obtained by calculating the two-time derivative of the distance as follows (see Appendix A for more details):

$$\bar{g}_{(x,s)} = \begin{pmatrix} \pi^2 s^2 g_x & 0 \\ 0^\top & \beta^2 \end{pmatrix}, \quad (7)$$

where  $g_x$  represents the metric of  $Z$  at  $x$ .

### 3.2.1. SCORE FUNCTION OF HIERARCHY

The Poincaré embedding defines an index, which is aimed to be an indicator of the hierarchical structure, that depends on the distance from the origin (8).

$$\text{score}(\text{is-a}(u, v)) = -(1 + \alpha(\|v\| - \|u\|))d(u, v) \quad (8)$$

This score function is penalized by the part after  $\alpha$ , so if  $v$  is closer to the origin than  $u$ , then it is easier to obtain larger values. In other words,  $v$  is higher in the hierarchy than  $u$  (i.e., “ $u$  is a  $v$ ” relationship holds). However, it is not appropriate to use this indicator for the Poincaré embedding. This model learns the embedding by maximizing this loss function:

$$L = \sum_{(u,v) \in E} \log \frac{\exp(-d_H(u, v))}{\sum_{v' \in N(u)} \exp(-d_H(u, v'))}, \quad (9)$$

where

$$d_H(x, y) := \text{arcosh} \left( 1 + \frac{\|x - y\|^2}{(1 - \|x\|^2)(1 - \|y\|^2)} \right). \quad (10)$$

This loss function only depends on the distance between the two embeddings. However, an isometric transformation in Poincaré ball exists, known as Möbius transformation ((Loustau, 2020)). Möbius transformation is defined as a map  $f : \mathbb{B}^n(\text{open unit ball}) \rightarrow \mathbb{B}^n$ , which can be written as a product of the inversions of  $\mathbb{R}^n (= \mathbb{R}^n \cup \{\infty\})$  through a sphere  $S$

that preserves  $\mathbb{B}^n$ . In contrast to Poincaré ball, the isometric transformation on the metric cone does not exist when the coordinate in the original space is fixed (we prove this property in Section 3.2.2). When we embed a graph into a metric cone, we define an indicator of the hierarchical structure by replacing the norm with a coordinate corresponding to the height of the cone (a one-dimensional parameter added to the original space). A point closer to the top of the cone is higher in the hierarchy. By analogy, a point closer to the bottom of the cone is lower in the hierarchy. Therefore, we have a natural indicator of the hierarchical structure.

### 3.2.2. IDENTIFIABILITY OF THE HEIGHTS IN CONE EMBEDDING

Let  $Z$  be an original embedding space (length metric space), and let  $X$  be a metric cone of  $Z$  with a parameter  $\beta > 0$ . We assume that each data point  $z_i \in Z$  ( $i = 1, \dots, n$ ) has its specific “height”  $t_i \in [0, 1]$  in the metric cone  $X$ . Our proposed method embeds data points into a metric cone based on the estimated distances  $\tilde{d}_\beta(x_i, x_j)$  ( $i, j = 1, \dots, n$ ) and tries to compute the heights  $t_1, \dots, t_n$  as a measure of the hierarchy level. However, it is not evident if these heights are identifiable only from the information of the original data points in  $Z$  and the distances  $\tilde{d}_\beta(x_i, x_j)$  ( $i, j = 1, \dots, n$ ) in the metric cone. The following theorem guarantees some identifiability.

**Theorem 1** (a) *Let  $n \geq 3$  and assume that  $z_1, \dots, z_n$  are not all aligned on a geodesic in  $Z$ . Then, the heights  $t_1, \dots, t_n$  are identifiable up to at most four candidates.*

(b) *Let  $n \geq 4$  and assume  $z_1, \dots, z_n$  and  $t_1, \dots, t_n$  take “general” positions and heights, respectively. Then, the heights  $t_1, \dots, t_n$  are identifiable uniquely.*

(c) *If  $d_Z(z_i, z_j) \geq \beta/2$  for all  $i, j = 1, \dots, n$ ,  $i \neq j$ , then the heights  $t_1, \dots, t_n$  are identifiable uniquely.*

A rigorous version of Theorem 1, including the precise meaning of “general” in (b), is explained in Appendix C. Theorem 1(a) indicates that the candidates of heights are finite, and we can expect the algorithm to converge to one of them, except for a very special data distribution in the original space  $Z$ . Moreover, by (b), even the uniqueness can be proved under very mild conditions. The statement in (c) implies that the uniqueness holds for arbitrary data distributions when we set  $\beta$  sufficiently small.

Remark that the assumption of “general” positions in Theorem 1 (b) is satisfied easily for most data distributions. For example, if both  $z_1, \dots, z_n \in \mathbb{R}^d$  and  $t_1, \dots, t_n \in [0, 1]$  are i.i.d. from a probability distribution whose density function exists with respect to the Lebesgue measure, then it is easy to see the assumption holds almost surely and therefore uniqueness of the solution is guaranteed. Note that for  $n = 3$  under the same setting, there can be multiple solutions with a positive probability.

### 3.2.3. USING PRETRAINED MODEL FOR COMPUTATIONAL EFFICIENCY AND SCALABILITY

Consider a situation where we already have a trained graph embedding on a Euclidean space (e.g., LINE), and we try to learn the embedding in a metric cone of the Euclidean space to extract information about the hierarchical structure. In this case, we can reduce the computational cost by fixing the coordinates corresponding to the original Euclidean space and learn only the one-dimensional parameters corresponding to heights in a metric cone added to the original space because the metric cone is one dimension larger than the original space. In addition, because the embedding in the original Euclidean space is preserved, it can be used as an input to the neural network (when the task considers information about the hierarchy, and the added one-dimensional parameters are also used as input) and can be easily applied to other tasks. However, other non-Euclidean embedding methods to extract hierarchical structures are not scalable because these methods cannot be applied directly to solve other tasks. For example, deep neural networks cannot use a non-Euclidean embedding as input because the sum of two vectors in the space and scalar product is not generally defined.

### 3.2.4. VARIABLE CURVATURE

One of the essences of Poincaré embedding is that a negative curvature of the Poincaré sphere is suitable for embedding tree graphs. The curvature of a metric cone has a similar property, i.e. a metric cone has a more negative curvature than the original space and, furthermore, the curvature can be controlled by hyperparameter  $\beta$ . We will verify these facts mathematically from two different aspects: (i) the scalar and the Ricci curvatures of a Riemannian manifold and (ii) the  $\text{CAT}(k)$  property of a length metric space.

First assume the original space  $\mathcal{M}$  is a  $n$ -dimensional Riemannian manifold with a metric  $g$ . Then the metric  $\tilde{g}$  of the corresponding metric cone with  $\beta$  can be defined except the apex and it becomes as (7). Let  $1, \dots, n$  be coordinate indices corresponding to  $x \in \mathcal{M}$  and 0 be the index corresponding to  $s \in [0, 1]$ . The Ricci curvatures  $\tilde{R}_{ij}$  and the scalar curvature  $\tilde{R}$  at  $(x, s)$  become

$$\tilde{R}_{\alpha\gamma} = R_{\alpha\gamma} - \pi^2(n-1)\beta^{-2}\tilde{g}_{\alpha\gamma}, \quad (11)$$

$$\tilde{R}_{\alpha 0} = \tilde{R}_{0\alpha} = \tilde{R}_{00} = 0, \quad (12)$$

$$\tilde{R} = \{\pi^{-2}R - n(n-1)\beta^{-2}\}s^{-2} \quad (13)$$

where  $\alpha, \gamma$  are coordinate indices in  $1, \dots, n$  and  $R_{ij}$  and  $R$  are the Ricci curvatures and the scalar curvature of  $\mathcal{M}$ , respectively. See the Appendix B for the derivation of such curvatures. The scalar curvature and the Ricci curvatures  $\tilde{R}_{\alpha\gamma}$  becomes more negative than (a constant times of) the original curvature for  $\beta < \infty$  and  $n \geq 2$ . Moreover, the smaller value of  $\beta$  makes the curvature more negative thus it becomes possible to control the curvature by tuning  $\beta$ . Note that the closer to the apex, i.e. the smaller the value of  $s$ , the greater the change of the scalar curvature.

Second assume the original space  $\mathcal{M}$  is a length metric space. This doesn't require a differentiable structure and is more general than the Riemannian manifold. In this case, we cannot argue the curvatures using the Riemannian metric but the  $\text{CAT}(k)$  property can be used instead. In (Kobayashi & Wynn, 2020), they proved the curvature of the metric cone is more negative or equal to the curvature of the original space and it can be controlled by  $\beta$  in the sense of the  $\text{CAT}(k)$  property.

## 4. Experiments

The claim in this paper is that ‘‘a hierarchical structure can be captured by adding a one-dimensional parameter and embedding it in a metric cone.’’ Therefore, we evaluate the proposed method in two experiments:

- embedding graphs (e.g., a social network);
- embedding taxonomies (e.g., WordNet).

As a comparison, we compare the proposed method with three other methods: Poincaré embedding, and ordinary embedding in Euclidean space, which are known to capture the hierarchical structure of graphs.

### 4.1. Embedding Graphs

Here, the accuracy of the metric cone embedding is evaluated by graph embedding. Following the experiments for Poincaré embedding in (Nickel & Kiela, 2017), we evaluate the proposed method on four networks of coauthors of research papers: ASTROPH, CONDMAT, GRQC, and HEPH. The graphs are designed so that each node represents a researcher. If there is a paper co-authored by two researchers, there is an edge between the corresponding nodes. In the graph embedding, all of the graph data are used for training, and the results are evaluated according to the accuracy with which the graph is reconstructed from the learned embedding. Because the same data are used for training and evaluation, we evaluate the fittingness of the embedding method to the data (not generalization performance).

The accuracy is calculated as follows:

1. Fix one node and calculate the distance to all other nodes. Sort the nodes in order of proximity.
2. Calculate the average of the rankings of neighboring nodes and the average precision.
3. Perform the above two operations on all the nodes and take the average.

The experimental results are shown in Table 1 and Table 2, where MR is the mean rank, and MAP is the mean average precision. The table confirms the effectiveness of the embedding method in a metric cone. See Appendix D for further experimental results.

Model	evaluation metric	GRQC				CONDMAT			
		10	20	50	100	10	20	50	100
Euclidean	MR	3.16	3.16	3.16	3.16	29.37	8.18	8.16	8.16
	MAP	0.999	0.999	0.999	0.999	0.745	0.990	0.996	0.997
Poincaré	MR	27.77	26.62	25.74	26.12	415.34	389.34	382.65	380.41
	MAP	0.879	0.881	0.883	0.882	0.721	0.727	0.729	0.729
Our Model (Metric Cone)	MR	3.16	3.16	3.16	3.16	27.85	8.18	8.16	8.16
	MAP	0.999	0.999	0.999	0.999	0.746	0.990	0.996	0.997

Table 1. MAP and rank score for Reconstruction and Link Prediction

Model	evaluation metric	ASTROPH				HEPPH			
		10	20	50	100	10	20	50	100
Euclidean	MR	117.67	29.43	3.83	3.83	14.11	2.73	2.61	2.61
	MAP	0.597	0.882	0.998	0.999	0.776	0.994	0.999	0.999
Poincaré	MR	671.59	654.60	641.54	637.66	194.23	190.90	189.09	188.60
	MAP	0.536	0.540	0.544	0.545	0.658	0.661	0.661	0.661
Our Model (Metric Cone)	MR	108.57	26.82	3.83	3.83	13.58	2.71	2.61	2.61
	MAP	0.611	0.885	0.998	0.999	0.775	0.994	0.999	0.999

Table 2. MAP and rank score for Reconstruction and Link Prediction

#### 4.2. Embedding Taxonomies

Following the Poincaré embedding, we evaluate the embedding accuracy of the hierarchical structure using WordNet. To verify this, we embed the nouns in WordNet into a metric cone and use the following score function, where the height in the cone is an indicator of hierarchy:

$$\text{score}(\text{is-a}((\mathbf{u}, s), (\mathbf{v}, t))) = -(1 + \alpha(s - t))d(\mathbf{u}, \mathbf{v}). \quad (14)$$

This score function is penalized by the part after  $\alpha$ , so if  $t$  is closer to the origin than  $s$ , then it is easier to obtain larger values. In other words,  $(v, t)$  is higher in the hierarchy than  $(u, s)$  (i.e., “ $(u, s)$  is a  $(v, t)$ ” relationship holds). In addition, the first term is used to avoid misjudging the relationship between the words with no relationship. Note that hyperparameter  $\alpha$  was set to  $10^3$ . The output of this score function and the correlation coefficient of the HyperLex dataset (Spearman’s  $\rho$ ) are used to evaluate the ability to represent the hierarchical structure of the model. The correlation coefficients and the embedding accuracy (mean rank (MR) and mean average precision (MAP)) are shown in Table 3. The table shows that our proposed model improves the score and captures the hierarchical structure better than other embedding methods.

Furthermore, an example visualization of the hierarchical structure of the embedding vectors obtained by the training is shown in Figure 2. As the figure illustrates, the closer the coordinate corresponding to the height in the cone is to zero (closer to the top of the cone), the higher the noun in the hierarchy is located in the embedded representation. For visualization, the embedding vectors in Euclidean space were reduced to two dimensions by principal component analysis.

		10	20	50	100
Euclidean	MR	1471.70	232.88	2.51	1.82
	MAP	0.070	0.122	0.838	0.899
Poincare	MR	19.94	19.62	19.47	19.36
	MAP	0.528	0.534	0.537	0.538
Our Model (Metric Cone)	MR	1401.28	209.11	2.30	1.79
	MAP	0.052	0.126	0.853	0.902
	corr	0.183	0.372	0.409	0.411

 Table 3. Embedding accuracy for WordNet (corr represents Spearman’s  $\rho$  on HYPERLEX)



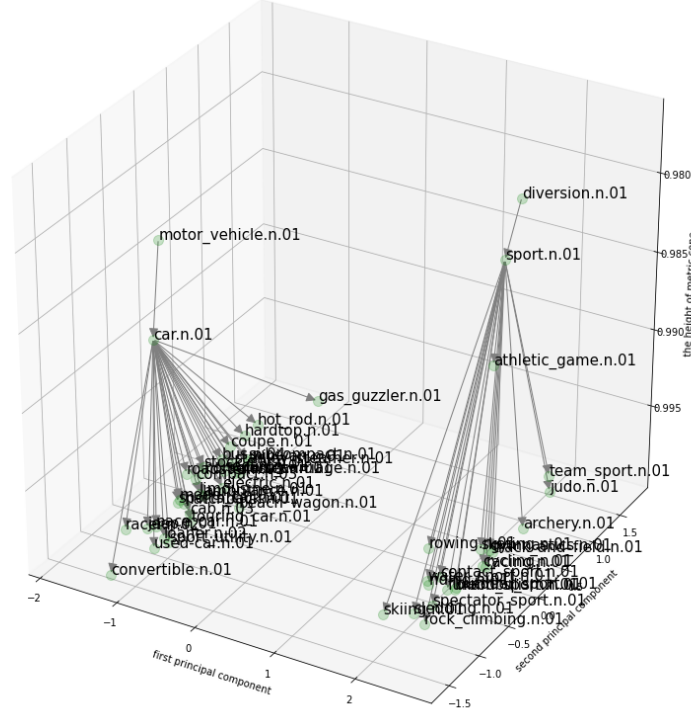


Figure 2. Visualization of WordNet Embedding using metric cone: each point is a word, and the two points connected by directed edges indicate that the word at the end of the arrow is a hyponym of the word at the start.

### 4.3. Hyperparameter optimization

In conducting experiments on our proposed method, we tuned the parameters  $\beta$  for batch size, number of epochs, number of negative samples, learning rate, and metric cone. For tuning, we performed a grid search on the HEPPH dataset, which is relatively small among the datasets used in this experiment, and trained on other graph datasets (GRQC, ASTROPH, CONDMAT) and WordNet using the tuned parameters. The tuning were conducted with the settings as follows:

- Batch sizes: 2048, 1024, 512, 256
- Number of epochs: 2000, 1500, 1000, 500
- Number of negative samples: 50, 20, 10, 5
- Learning rate: 100.0, 10.0, 1.0, 0.1
- Metric cone parameters  $\beta$ : 50, 10, 1, 0.1

Based on the results of the search with these settings, the experiments with the results in the table are Batch size: 256, number of epochs: 2000, number of negative samples: 50, learning rate: 10.0(in embedding graphs) and 1.0(in embedding taxonomies), beta: 50. As for the batch size, the number of epochs, and the number of negative samples, as with the tuning of a normal neural network, the smaller the batch size, the larger the number of epochs, and the larger the number of negative samples, the better the results. As for the learning rate, due to the sparse size of the dataset used in this study, we were able to obtain better results by varying the learning rate according to the data. The experimental results of our proposed method were highly dependent on  $\beta$ , the parameter of the metric cone. One possible reason for this is that by fixing  $\beta$ , the distance between two points in space is upper-bounded:

$$d_{\beta}((x, s), (y, t)) \leq 2\beta. \quad (15)$$



The curvature of the data space needs to be optimized in order to embed a graph data efficiently, since the curvature of the space changes with  $\beta$ . Remark that by (12) and (13), the effect of changes of parameter  $\beta$  on the Ricci and the scalar curvatures is greater if the original space has higher dimensions. Therefore, delicate tuning of the parameters  $\beta$  is required, especially in the case of high dimensions.

## 5. discussion and future works

In this study, we have demonstrated that a graph embedding in a metric cone that is a dimension larger than the existing embedding methods has the following advantages: 1) we naturally define an index (score function) as an indicator of hierarchy, 2) we improve computational efficiency and scalability to various tasks, and 3) we enhance accuracy by changing the curvature.

Future research topics include 1) efficient optimization of curvature, 2) development of an embedding method to update existing embeddings in learning, and 3) discovery of applications to other tasks. In this study, we measured the improvement of the accuracy of curvature optimization by the grid search. However, more efficient methods, such as gradient-based methods, can be used to optimize the embedding space. We also learned embedding in a metric cone under the constraint of not updating existing embeddings. We learned embedding for a metric cone that was randomly initialized; however, the training accuracy was not satisfactory. One possible reason for this is that optimization in metric cones is difficult and tends to fall into local solutions. Therefore, to optimize the entire embedding, an efficient method of optimizing functions on a metric cone (or Riemannian manifold) should be developed in future work.

## 6. Acknowledgement

The idea of applying metric cones to data science was born during a collaboration with Henry P. Wynn.

## References

- Abu-El-Haija, S., Perozzi, B., Al-Rfou, R., and Alemi, A. A. Watch your step: Learning node embeddings via graph attention. In *Advances in Neural Information Processing Systems*, pp. 9180–9190, 2018.
- Belkin, M. and Niyogi, P. Laplacian eigenmaps and spectral techniques for embedding and clustering. In *Advances in neural information processing systems*, pp. 585–591, 2002.
- Bordes, A., Usunier, N., Garcia-Duran, A., Weston, J., and Yakhnenko, O. Translating embeddings for modeling multi-relational data. In *Advances in neural information processing systems*, pp. 2787–2795, 2013.
- Cao, S., Lu, W., and Xu, Q. Deep neural networks for learning graph representations. In *AAAI*, volume 16, pp. 1145–1152, 2016.
- Cox, D., Little, J., and OShea, D. *Ideals, varieties, and algorithms: an introduction to computational algebraic geometry and commutative algebra*. Springer Science & Business Media, 2013.
- Deza, M. M. and Deza, E. Encyclopedia of distances. In *Encyclopedia of distances*, pp. 1–583. Springer, 2009.
- Ganea, O., Becigneul, G., and Hofmann, T. Hyperbolic entailment cones for learning hierarchical embeddings. volume 80 of *Proceedings of Machine Learning Research*, pp. 1646–1655, Stockholmsmässan, Stockholm Sweden, 10–15 Jul 2018. PMLR. URL <http://proceedings.mlr.press/v80/ganea18a.html>.
- Grover, A. and Leskovec, J. node2vec: Scalable feature learning for networks. In *Proceedings of the 22nd ACM SIGKDD international conference on Knowledge discovery and data mining*, pp. 855–864, 2016.
- Hoff, P. D., Raftery, A. E., and Handcock, M. S. Latent space approaches to social network analysis. *Journal of the american Statistical association*, 97(460):1090–1098, 2002.
- Janson, S. Riemannian geometry: some examples, including map projections. *Notes*, 2015. URL <http://www2.math.uu.se/~svante/papers/sjN15.pdf>.
- Kipf, T. N. and Welling, M. Variational graph auto-encoders. *NIPS Workshop on Bayesian Deep Learning*, 2016.

- Kipf, T. N. and Welling, M. Semi-supervised classification with graph convolutional networks. In *International Conference on Learning Representations (ICLR)*, 2017.
- Klimovskaia, A., Lopez-Paz, D., Bottou, L., and Nickel, M. Poincaré maps for analyzing complex hierarchies in single-cell data. *Nature Communications*, 11(1):1–9, 2020.
- Kobayashi, K. and Wynn, H. P. Empirical geodesic graphs and cat (k) metrics for data analysis. *Statistics and Computing*, 30(1):1–18, 2020.
- Kruskal, J. B. Multidimensional scaling by optimizing goodness of fit to a nonmetric hypothesis. *Psychometrika*, 29(1): 1–27, 1964.
- Loustau, B. Hyperbolic geometry. *arXiv preprint arXiv:2003.11180*, 2020.
- Mikolov, T., Sutskever, I., Chen, K., Corrado, G. S., and Dean, J. Distributed representations of words and phrases and their compositionality. In *Advances in neural information processing systems*, pp. 3111–3119, 2013.
- Nickel, M. and Kiela, D. Poincaré embeddings for learning hierarchical representations. In *Advances in neural information processing systems*, pp. 6338–6347, 2017.
- Nickel, M. and Kiela, D. Learning continuous hierarchies in the Lorentz model of hyperbolic geometry. volume 80 of *Proceedings of Machine Learning Research*, pp. 3779–3788, Stockholmsmässan, Stockholm Sweden, 10–15 Jul 2018. PMLR. URL <http://proceedings.mlr.press/v80/nickel18a.html>.
- Perozzi, B., Al-Rfou, R., and Skiena, S. Deepwalk: Online learning of social representations. In *Proceedings of the 20th ACM SIGKDD international conference on Knowledge discovery and data mining*, pp. 701–710, 2014.
- Roweis, S. T. and Saul, L. K. Nonlinear dimensionality reduction by locally linear embedding. *science*, 290(5500): 2323–2326, 2000.
- Sturm, K.-T. Probability measures on metric spaces of nonpositive. *Heat Kernels and Analysis on Manifolds, Graphs, and Metric Spaces: Lecture Notes from a Quarter Program on Heat Kernels, Random Walks, and Analysis on Manifolds and Graphs: April 16-July 13, 2002, Emile Borel Centre of the Henri Poincaré Institute, Paris, France*, 338:357, 2003.
- Tang, J., Qu, M., Wang, M., Zhang, M., Yan, J., and Mei, Q. Line: Large-scale information network embedding. In *Proceedings of the 24th international conference on world wide web*, pp. 1067–1077, 2015.
- Tenenbaum, J. B., De Silva, V., and Langford, J. C. A global geometric framework for nonlinear dimensionality reduction. *science*, 290(5500):2319–2323, 2000.
- Wang, D., Cui, P., and Zhu, W. Structural deep network embedding. In *Proceedings of the 22nd ACM SIGKDD international conference on Knowledge discovery and data mining*, pp. 1225–1234, 2016.

## Appendix

### A. Derivation of the metric tensor of a metric cone

Let  $\mathcal{M}$  be an  $n$ -dimensional Riemannian manifold with a metric  $g$ . Then the metric  $\bar{g}$  of the corresponding metric cone  $\tilde{\mathcal{M}} = \tilde{\mathcal{M}}_\beta$  can be defined except the apex. Denote the square of the infinitesimal distance in  $\tilde{\mathcal{M}}$  as  $|d\tilde{s}|^2$ , then

$$\begin{aligned}
 |d\tilde{s}|^2 &= \bar{d}_\beta((x, r), (x + dx, r + dr))^2 \\
 &= \beta^2 (2r^2 + 2rdr + dr^2 - 2(r + dr)r \cos(\pi \min(d_{\mathcal{M}}(x, x + dx)/\beta, 1))) \\
 &\approx \beta^2 \left( 2r^2 + 2rdr + dr^2 - 2(r^2 + rdr) \left( 1 - \frac{(\pi d_{\mathcal{M}}(x, x + dx)/\beta)^2}{2} \right) \right) \\
 &\approx \beta^2 dr^2 + \pi^2 r^2 \sum_{i,j} g_{ij} dx_i dx_j + \pi^2 r dr \sum_{i,j} g_{ij} dx_i dx_j \\
 &\approx \begin{pmatrix} dx \\ dr \end{pmatrix}^\top \begin{pmatrix} \pi^2 r^2 g_{ij} & 0 \\ 0 & \beta^2 \end{pmatrix} \begin{pmatrix} dx \\ dr \end{pmatrix}.
 \end{aligned} \tag{16}$$

Therefore, the metric tensor  $\bar{g}$  becomes

$$\bar{g} = \begin{pmatrix} r^2 \pi^2 g & 0 \\ 0 & \beta^2 \end{pmatrix}. \tag{17}$$

### B. Derivation of the Ricci and the scalar curvatures of a metric cone

We will derive the Ricci and scalar curvatures of metric cone  $\tilde{\mathcal{M}}$ . Let  $0, 1, \dots, n$  be the coordinate indices of metric cone  $\tilde{\mathcal{M}}$  where 0 corresponds to the radial coordinate  $s \in (0, 1)$  and  $1, \dots, n$  correspond to  $x \in \mathcal{M}$ .

**Claim 2** *The Ricci curvatures  $\tilde{R}_{ij}$  and the scalar curvature  $\tilde{R}$  become*

$$\begin{aligned}
 \tilde{R}_{\alpha\gamma} &= R_{\alpha\gamma} - \pi^2(n-1)\beta^{-2}g_{\alpha\gamma}, \tilde{R}_{\alpha 0} = \tilde{R}_{0\alpha} = \tilde{R}_{00} = 0, \\
 \tilde{R} &= \{\pi^{-2}R - n(n-1)\beta^{-2}\}s^{-2}
 \end{aligned} \tag{18}$$

where  $\alpha$  and  $\gamma$  are coordinate indices in  $1, \dots, n$  and  $R_{ij}$  and  $R$  are the Ricci curvatures and the scalar curvature of  $\mathcal{M}$ , respectively.

**Proof.** By Example 4.6 of (Janson, 2015), if the metric of  $\tilde{\mathcal{M}}$  is defined by the squared infinitesimal distance  $|ds|^2$  in  $\mathcal{M}$  and a  $\mathcal{C}^2$ -class function  $w$  on an open interval  $J \subset \mathbb{R}$  as

$$|d\tilde{s}|^2 = \beta^2 |dr|^2 + w(r)^2 |ds|^2, \tag{19}$$

the Ricci curvature tensor becomes

$$\begin{aligned}
 \tilde{R}_{\alpha\gamma} &= R_{\alpha\gamma} - \left( (n-1) \left( \frac{w'}{w} \right)^2 + \frac{w''}{w} \right) \tilde{g}_{\alpha\gamma} \\
 &= R_{\alpha\gamma} - \left( (n-1) \left( \frac{w'}{w} \right)^2 + \frac{w''}{w} \right) w^2 g_{\alpha\gamma},
 \end{aligned} \tag{20}$$

$$\tilde{R}_{\alpha 0} = 0, \quad \tilde{R}_{00} = -(n-1) \frac{w''}{w} \tag{21}$$

and the scalar curvature becomes

$$\tilde{R} = w^{-2}(R - n(n-1)(w')^2 - 2nww''). \quad (22)$$

Since the metric of a metric cone  $\tilde{M}$  is given by

$$|d\tilde{s}|^2 = \beta^2 |dr|^2 + \pi^2 r^2 |ds|^2, \quad (23)$$

by setting  $\tilde{r} := \beta r$  and  $w(\tilde{r}) := \pi\beta^{-1}\tilde{r}$ , we obtain the following form similar to (19):

$$|d\tilde{s}|^2 = |d\tilde{r}|^2 + w(\tilde{r})^2 |ds|^2. \quad (24)$$

By substituting  $w(\tilde{r}) = \pi\beta^{-1}\tilde{r} = \pi r$ ,  $w'(\tilde{r}) = \pi\beta^{-1}$  and  $w''(\tilde{r}) = 0$ , we obtain the Ricci and scalar curvatures in Claim 2  $\square$

### C. Identifiability of the hights in the cone embedding

In this section, we will prove Theorem 1 of the main article. Let us begin by rewriting Theorem 1 as a longer but more theoretically rigorous form.

**Theorem 3 (A rigorous restatement of Theorem 1)** *Let  $Z$  be a length metric space and  $X$  be a metric cone of  $Z$  with a parameter  $\beta > 0$ . Let  $n$  be an integer at least 3. Fix  $z_i \in Z$  and  $x_i := (z_i, t_i) \in X$  with  $t_i \in [0, 1]$  for  $i = 1, \dots, n$ . Denote a matrix  $\tilde{D} := [\tilde{d}_\beta(x_i, x_j)]_{i,j=1}^n$ .*

- (a) *Assume  $z_1, \dots, z_n$  are not all aligned in a geodesic. Given  $z_1, \dots, z_n$  and  $\tilde{D}$ , the number of possible values of  $(t_1, \dots, t_n)$  is at most four.*
- (b) *Let  $n \geq 4$  and assume  $z_1, \dots, z_n$  and  $t_1, \dots, t_n$  are in a “general” position. Here “general” position means that, besides the assumption in (a), given any distinct 4 points  $z_i, z_j, z_k, z_l \in Z$  and corresponding heights  $t_i, t_j, t_k \in [0, 1]$ , but still  $t_l$  can take infinitely many values. Then  $t_1, \dots, t_n$  are determined uniquely by  $z_1, \dots, z_n$  and  $\tilde{D}$ .*
- (c) *If  $d(z_i, z_j) \geq \beta/2$  for all  $i, j = 1, \dots, n$ ,  $i \neq j$ , then  $t_1, \dots, t_n$  are determined uniquely by  $z_1, \dots, z_n$  and  $\tilde{D}$ .*

Before the proof, we will state some remarks.

If  $n = 2$ , the identifiability problem reduces to an elementary geometric question: given a circle sector as the right two subfigures of Figure 1 of the main paper and the length of the blue line segment(s) connecting  $(x, s)$  and  $(y, t)$ , can  $s$  and  $t$  be determined uniquely? The answer is evidently no. But it is notable that there are two types of counterexamples. The first type is as Figure 3(A), one point moves “up” and the other moves “down”. The other type as Figure 3(B) is maybe counter-intuitive: both moves “up” or “down”. Note that the second case does not happen if the angle  $\theta$  is larger than or equal to  $\pi/2$ .

If  $n = 3$ , the picture becomes a tetrahedron as in Figure 4. Here the angles and edge lengths are defined by

$$\begin{aligned} \theta_1 &:= \pi \min(d_Z(z_2, z_3)/\beta, 1), & a_1 &:= \tilde{d}_\beta(x_2, x_3) \\ \theta_2 &:= \pi \min(d_Z(z_3, z_1)/\beta, 1), & a_2 &:= \tilde{d}_\beta(x_3, x_1) \\ \theta_3 &:= \pi \min(d_Z(z_1, z_2)/\beta, 1), & a_3 &:= \tilde{d}_\beta(x_1, x_2) \end{aligned} \quad (25)$$

and  $\theta_1 + \theta_2 + \theta_3$  is assumed to be at most  $2\pi$ . Then the geometrical question becomes “when angles  $\alpha, \beta, \gamma$  and edge lengths  $a_1, a_2, a_3$  of triangle  $\triangle x_1 x_2 x_3$  is given, can the position of the points  $x_1, x_2$  and  $x_3$  be determined uniquely?” If it is not unique and there are two different positions of  $x_1, x_2$  and  $x_3$ , at least one edge should move as in Figure 3(B) since it is impossible to move all the three edges as in Figure 3(A). But if all of the angles are larger than or equal to  $\pi/2$ , this cannot happen. This gives actually a geometrical proof of Theorem 3 (c).

If  $\theta_1 + \theta_2 + \theta_3$  is larger than  $2\pi$ , the geometric arguments become complicated. We do not need this kind of case analysis when we use algebraic arguments as in the following proof.

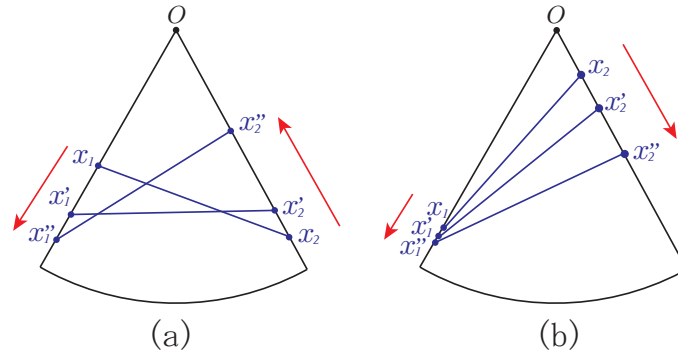


Figure 3. Two types of movement for a line segment of constant length

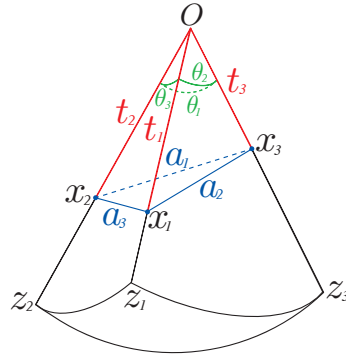


Figure 4. Metric cone generated by three points  $z_1, z_2, z_3 \in Z$

Now we will prove the theorem. In the proof, we use the Gröbner basis as a tool of computational algebra. See for example (Cox et al., 2013) about definition and application of the Gröbner basis.

**Proof.** (a) Since the maximum number of possible values of  $(t_1, \dots, t_n)$  does not increase with  $n$ , it is enough to prove for  $n = 3$ . We set  $\theta_1, \theta_2, \theta_3 \in [0, \pi]$  and  $a_1, a_2, a_3 \geq 0$  as (25). Then by the law of cosine,

$$\begin{aligned} t_2^2 + t_3^2 - 2t_2t_3 \cos \theta_1 &= a_1^2, \\ t_3^2 + t_1^2 - 2t_3t_1 \cos \theta_2 &= a_2^2, \\ t_1^2 + t_2^2 - 2t_1t_2 \cos \theta_3 &= a_3^2. \end{aligned} \quad (26)$$

We consider this as a system of polynomial equations with variables  $t_1, t_2, t_3$  and compute the Gröbner basis of the ideal generated by the corresponding polynomials by degree lexicographic monomial order (deglex) with  $t_1 > t_2 > t_3$  by Mathematica. Then the output becomes as in Note 6 and the basis includes  $-t_1^2 + (2 \cos \theta_2)t_1t_3 - t_3^2 + a_2^2$ ,  $-t_2^2 + (2 \cos \theta_3)t_2t_3 - t_3^2 + a_3^2$  and  $4v(\theta_1, \theta_2, \theta_3)t_3^4 + (\text{terms of degree} \leq 2)$  where

$$v(\theta_1, \theta_2, \theta_3) := 1 + 2 \cos \theta_1 \cos \theta_2 \cos \theta_3 - \cos^2 \theta_1 - \cos^2 \theta_2 - \cos^2 \theta_3. \quad (27)$$

Note that when  $\theta_1 + \theta_2 + \theta_3 \leq 2\pi$ ,  $\frac{a_1 a_2 a_3}{6} v(\theta_1, \theta_2, \theta_3)$  is a formula of the volume of the tetrahedron whose base triangle is  $\triangle x_1 x_2 x_3$  and, therefore, it has a positive value unless the tetrahedron degenerates. By the assumption,  $z_1, z_2, z_3$  are not aligned in a geodesic and therefore the tetrahedron does not degenerate and  $v(\theta_1, \theta_2, \theta_3)$  must be nonzero. Note that this becomes negative when  $\theta_1 + \theta_2 + \theta_3 > 2\pi$ .

On the other hand, it is known that the system of polynomial equations with a Gröbner basis  $G$  has a finite number of (complex) solutions if and only if, for each variable  $x$ ,  $G$  contains a polynomial with a leading monomial that is a power of  $x$ . Now all variables  $t_1, t_2$  and  $t_3$  satisfy such property, thus we conclude there are at most a finite number of solutions.

Then by Bézout's theorem, the number of solutions is at most the product of the degree of three polynomial equations, i.e.  $2 \times 2 \times 2 = 8$ . But if  $(t_1, t_2, t_3)$  is a solution,  $(-t_1, -t_2, -t_3)$  is also a solution, and only one of each pair can satisfy  $t_1, t_2, t_3 \leq 0$ . Thus we conclude the number of possible values of  $(t_1, t_2, t_3)$  is at most four.

(b) By the assumptions in (a), without loss of generality, we can assume  $z_1, z_2, z_3$  are not aligned in a geodesic. By the result of (a), given  $z_1, z_2, z_3$  and distances  $\tilde{d}_\beta(x_1, x_2), \tilde{d}_\beta(x_1, x_3), \tilde{d}_\beta(x_2, x_3)$ , there are at most four variations of the values of  $(t_1, t_2, t_3)$ . Here we assume  $t_1$  can take multiple values including  $\hat{t}_1$  and  $\check{t}_1$ .

Suppose, in addition to the above, the values of  $z_4$  and  $\tilde{d}_\beta(x_1, x_4)(= a_4)$  are given and let  $\theta_4 := \pi \min(d_Z(z_1, z_4)/\beta, 1)$ . Then both  $\hat{t}_1$  and  $\check{t}_1$  satisfy  $t_1^2 + t_4^2 - 2t_1t_4 \cos \theta_4 = a_4^2$  and therefore  $2t_4 \cos \theta_4 = \hat{t}_1 + \check{t}_1$  must hold. Since  $\hat{t}_1$  and  $\check{t}_1$  are different non-negative values,  $\hat{t}_1 + \check{t}_1 > 0$  and, therefore,  $\cos \theta_4 \neq 0$ . Hence we obtain  $t_4 = (\hat{t}_1 + \check{t}_1)/2 \cos \theta$ .

This means if  $t_4$  takes values except  $(\hat{t}_1 + \check{t}_1)/2 \cos \theta$ , at most only one of  $\hat{t}_1$  and  $\check{t}_1$  can be a solution. We can reduce each pairwise ambiguity of the (at most) 4 possibilities of  $(t_1, t_2, t_3)$  one by one similarly. Finally  $(t_1, t_2, t_3)$  are determined uniquely for all except at most  $\binom{4}{2} = 6$  values of  $t_4$ . But such finite values of  $t_4$  can be neglected thanks to the assumption of "general" position in the theorem. Since the same argument holds for any triplets, the statement has been proved.

(c) If  $(t_1, \dots, t_n)$  can take multiple values, without loss of generality we can assume  $(t_1, t_2, t_3)$  takes multiple values. By the assumption in the theorem,  $\theta_1, \theta_2, \theta_3 \geq \pi/2$  and therefore all coefficients in each equation of (26) become positive. Thus, if  $t_i$  increases/decreases then  $t_j$  must decrease/increase for  $(i, j) = (1, 2), (2, 3), (3, 1)$  but this cannot happen simultaneously. Hence  $(t_1, t_2, t_3)$  cannot take multiple values.

Note that all of this proof works even when  $\theta_1 + \theta_2 + \theta_3$  is larger than  $2\pi$ .  $\square$

**Remark 4** Assumption in Theorem 3 (a) is necessary. If the assumption fails, the tetrahedron degenerates and  $x_1, x_2, x_3$  and the apex  $O$  are all in a plane. When  $O$  happens to be on a circle passing through  $x_1, x_2$  and  $x_3$ , move  $O$  to another point  $O'$  on the same circle. Then the angles corresponding to  $\theta_1, \theta_2, \theta_3$  do not change by the inscribed angle theorem. By an elemental geometrical argument, a new position of  $x_1, x_2, x_3$  and  $O'$  gives another solution of  $t_1, t_2, t_3$ . Hence obviously there are infinite number of solutions.

**Remark 5** The assumption of “general” positions of  $z_1, \dots, z_n$  in Theorem 3 (b) is satisfied easily for most data distributions. For example, if both  $z_1, \dots, z_n \in \mathbb{R}^d$  and  $t_1, \dots, t_n \in [0, 1]$  are i.i.d. from a probability distribution whose density function exists with respect to the Lebesgue measure, then it is easy to see the assumption holds almost surely and therefore uniqueness of the solution is guaranteed. Note that for  $n = 3$  under the same setting, there can be multiple solutions with a positive probability.

**Note 6** Computation of the Gröbner basis by Mathematica:

For simplicity, we put  $x := t_1$ ,  $y := t_2$ ,  $z := t_3$ ,  $a := 2 \cos \theta_1$ ,  $b := 2 \cos \theta_2$ ,  $c := 2 \cos \theta_3$ ,  $d := a_1^2$ ,  $e := a_2^2$  and  $f := a_3^2$ .

Note that the second, first and last polynomials in the output correspond to  $-t_1^2 + (2 \cos \theta_2)t_1t_3 - t_3^2 + a_2^2$ ,  $-t_2^2 + (2 \cos \theta_3)t_2t_3 - t_3^2 + a_3^2$  and  $4v(\theta_1, \theta_2, \theta_3)t_3^4 + (\text{terms of degree } \leq 2)$  in the proof, respectively.

```
-----
In := GroebnerBasis[{x^2 + y^2 - a*x*y - d, x^2 + z^2 - b*x*z - e,
  y^2 + z^2 - c*y*z - f}, {x, y, z},
  MonomialOrder -> DegreeLexicographic]

Out = {f - y^2 + c y z - z^2, e - x^2 + b x z - z^2,
  d - x^2 + a x y - y^2,
  d x - e x + a e y - x y^2 - b d z + b y^2 z + x z^2 -
  a y z^2, -c d x + c e x - a c e y + b f y + c x y^2 - b y^3 +
  b c d z - a f z + a y^2 z - c x z^2 - b y z^2 + a z^3,
  a f x + d y - f y - x^2 y - c d z + c x^2 z - a x z^2 + y z^2,
  b f x - c e y + c x^2 y - b x y^2 + e z - f z - x^2 z +
  y^2 z, -c e x + a b f x + c x^3 + b d y - b f y - b x^2 y -
  b c d z + a e z - a x^2 z + c x z^2 + b y z^2 - a z^3,
  a c d x - a c e x + b f x + c d y - c e y + a^2 c e y - a b f y -
  b x y^2 + a b y^3 - c y^3 - a b c d z + e z - f z + a^2 f z -
  x^2 z + y^2 z - a^2 y^2 z + a c x z^2 + a b y z^2 -
  a^2 z^3, -a e f - d x y + e x y + f x y + c d x z - c e x z +
  b d y z - b f y z - b c d z^2 + a e z^2 + a f z^2 - 2 x y z^2 +
  c x z^3 + b y z^3 - a z^4, -c d e + c e^2 - a b e f + c d x^2 -
  c e x^2 - b d x y + b e x y + b f x y - a f x z - d y z +
  b^2 d y z + 2 e y z + f y z - b^2 f y z - x^2 y z + 2 c d z^2 -
  b^2 c d z^2 + a b e z^2 - 2 c e z^2 + a b f z^2 + a x z^3 -
  3 y z^3 + b^2 y z^3 - a b z^4 + c z^4, -d x + a^2 d x + a b c d x +
  2 e x - a^2 e x - a b c e x - a^2 f x + b^2 f x - x^3 + b c d y -
  a e y + a^3 e y - b c e y + a^2 b c e y + a f y - a b^2 f y +
  x y^2 - b^2 x y^2 - a y^3 + a b^2 y^3 - b c y^3 + b d z -
  a^2 b d z + a c d z - a b^2 c d z + b e z - a c e z - b f z +
  a^2 b f z - 2 x z^2 + 2 a^2 x z^2 - a^3 y z^2 + a b^2 y z^2 -
  a^2 b z^3 + a c z^3, -c d^2 + c d e + a b d f + c d x^2 - c e x^2 +
  b f x y - a b d y^2 + 2 c d y^2 - 2 c e y^2 + a^2 c e y^2 -
  a b f y^2 - b x y^3 + a b y^4 - c y^4 - a d x z + a e x z -
  a f x z - 2 d y z + e y z - a^2 e y z - f y z + a^2 f y z +
  x^2 y z + 3 y^3 z - a^2 y^3 z,
  d^2 - 2 d e + c^2 d e + e^2 - c^2 e^2 - 2 d f + b^2 d f + 2 e f -
  a^2 e f + a b c e f + f^2 - b^2 f^2 - c^2 d x^2 + c^2 e x^2 +
  b c d x y - b c e x y - b c f x y - b^2 d y^2 + b^2 f y^2 +
  a c d x z - a c e x z + a c f x z + a b d y z + a b e y z -
  a b f y z + 4 d z^2 - 2 b^2 d z^2 - a b c d z^2 - 2 c^2 d z^2 +
  b^2 c^2 d z^2 - 4 e z^2 + a^2 e z^2 - a b c e z^2 + 2 c^2 e z^2 -
  4 f z^2 + a^2 f z^2 + 2 b^2 f z^2 - a b c f z^2 + 4 z^4 - a^2 z^4 -
  b^2 z^4 + a b c z^4 - c^2 z^4}
```

## D. Additional results on the metric cone embedding

In this section, we will examine how the learning of embedding in a metric cone proceeds. We will use the GrQc dataset, which is the smallest dataset used in the paper. The experiments were conducted by learning the Euclidean embedding and the metric-cone embedding for 2-9 dimensions. The hyperparameters were set as in the paper:



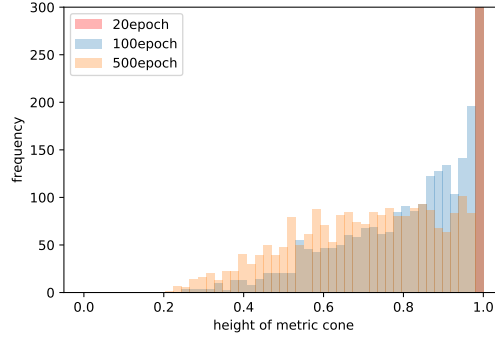


Figure 5. Changes in the distribution of the heights of data points: The smaller the x axes, the higher the point embedded in the metric cone. For visualization, the display of y-axis is limited between 0 and 300.

- Learning rate: 10.0
- Epoch: 2000
- Negative sampling rate: 50
- Batch size: 256.

The ratio of the scaling of the original space  $\mathcal{M}$ , which is an Euclidean space for now, and the value of parameter  $\beta$  affects the accuracy of the metric-cone learning significantly. Since the distance between two points in a metric cone is bounded by a constant times  $\beta$ , we set  $\beta$  as the maximum norm of the embedding in the original Euclidean space. All initial values of the height are set as 1.

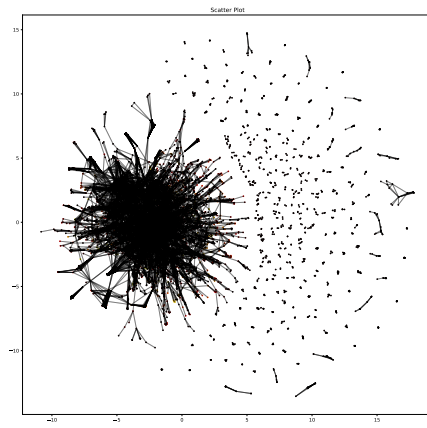
Model	evaluation metric	2	3	4	5	6	7	8	9
Euclidean	MR	88.99	37.17	17.15	9.42	5.78	4.27	3.42	3.18
	MAP	0.375	0.488	0.600	0.719	0.842	0.929	0.983	0.998
Our Model (Metric Cone)	MR	72.35	26.39	14.50	8.65	5.50	4.16	3.40	3.18
	MAP	0.450	0.551	0.614	0.726	0.851	0.935	0.986	0.998

Table 4. Results of GrQc embedding into low-dimensional space

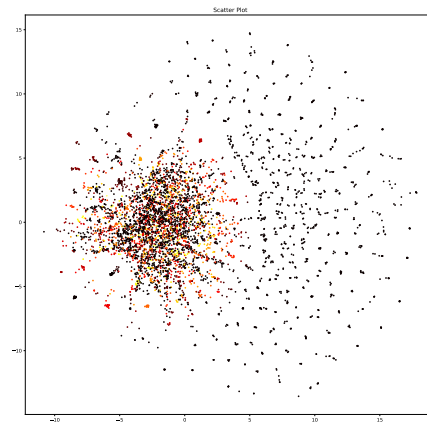
Table 4 shows the experimental results. In the experiments using GrQc in the paper, learning in the original Euclidean embedding was close to overfitting, so there was almost no difference in the accuracy between the Euclidean embedding and the metric-cone embedding. On the other hand, when the training accuracy of the Euclidean embedding does not hit the ceiling, the embedding in a metric cone can improve the test accuracy. In other words, the embedding into a metric cone can represent the hierarchical structure of the data more efficiently.

Figure 5 shows how the distribution of the heights of the data points in a metric cone changes as the learning progresses. For visualization of the embedding after 20 epoch (equal to the Euclidean embedding), 100 epoch, and 500 epoch training.

Figure 6 is a visualization of the distribution of the heights of data. The embedding vectors in Euclidean space were reduced to two dimensions by PCA. From the figure, it can be seen that as the learning progresses, the points closer to the center of the dense area gradually move toward the top of the cone.



(a) The Euclidean embedding and edges



(b) The Euclidean embedding and the heights computed by the metric-cone embedding

*Figure 6.* Visualization of the distribution of the heights of data by PCA: The color of each data point represents its height, i.e. the brighter the color, the closer to the top of the cone (closer to 0).